POLITECNICO DI TORINO
Repository ISTITUZIONALE

Reservoir Effects on Flood Peak Discharge at the Catchment Scale

Original
Reservoir Effects on Flood Peak Discharge at the Catchment Scale / Volpi, E., Di Lazzaro, M., Bertola, M., Viglione, A., Fiori, A.. - In: WATER RESOURCES RESEARCH. - ISSN 0043-1397. - 54:11(2018), pp. 9623-9636. [10.1029/2018WR023866]

Availability:
This version is available at: 11583/2728011 since: 2020-01-30T15:59:43Z

Publisher:
AGU Wiley

Published
DOI:10.1029/2018WR023866

Terms of use:

This article is made available under terms and conditions as specified in the corresponding bibliographic description in the repository

Publisher copyright

(Article begins on next page)

08 October 2026

AGU100 ADVANCING EARTH AND SPACE SCIENCE

Water Resources Research

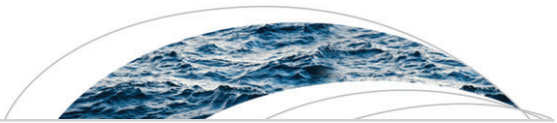

RESEARCH ARTICLE
10.1029/2018WR023866

Reservoir Effects on Flood Peak Discharge at the Catchment Scale

E. Volpi[1], M. Di Lazzaro[1], M. Bertola[2], A. Viglione[2], and A. Fiori[1]

[1]Department of Engineering, Roma Tre University, Rome, Italy, [2]Institute of Hydraulic Engineering and Water Resources Management, Vienna University of Technology, Vienna, Austria

Key Points:
- We propose a method to easily quantify reservoirs attenuation on downstream flood frequency curve
- Flood peak attenuation is mainly controlled by reservoir position within the catchment, spillway dimensions, and storage capacity
- Optimal positions exist that maximize flood peak attenuation and are generally different from catchment outlet

Correspondence to:
E. Volpi,
elena.volpi@uniroma3.it

Citation:
Volpi, E., Di Lazzaro, M., Bertola, M., Viglione, A., & Fiori, A. (2018). Reservoir effects on flood peak discharge at the catchment scale. *Water Resources Research*, *54*, 9623–9636. https://doi.org/10.1029/2018WR023866

Received 8 AUG 2018
Accepted 12 NOV 2018
Accepted article online 19 NOV 2018
Published online 29 NOV 2018

The copyright line for this article was changed on 4 DEC 2019 after original online publication.

Abstract This paper proposes a method to easily quantify the attenuation due to a reservoir on downstream flood peak discharges, that is, to the downstream flood frequency curve. Using a parsimonious Instantaneous Unit Hydrograph-based model, we show that the flood peak attenuation is mainly controlled by three system characteristics: (1) the reservoir position along the river channel, (2) the spillway dimensions, quantified by the reservoir storage coefficient; and (3) the storage capacity. These three system characteristics are quantified by three dimensionless numbers, which are derived analytically for an idealized catchment. The degree of flood peak attenuation increases for increasing storage capacity and spillway dimensions, in different ways depending on the reservoir position along the river channel. An optimal position exists, which maximizes the degree of flood peak attenuation, and is in general different from the outlet of the catchment. Interestingly, for large reservoirs with relatively small spillways, a range of quasi-optimal positions exists. With the Instantaneous Unit Hydrograph-based model, we also investigate how the duration of extreme rainfall relevant for determining the maximum flood peaks at the catchment outlet changes depending on the three system characteristics. Some of the assumptions of the method (i.e., catchment simple morphology and linearity of reservoir response) are relaxed in a real-world example, which demonstrates that the synthetic results approximate well what would be obtained by a more realistic model.

1. Introduction

The regulation of rivers with reservoirs is meant to alter the natural flow regime by storing and releasing water volumes, with specific operation rules, in order to meet human needs (e.g., irrigation, water supply, hydropower, flood control, and recreational use). These alterations determine several impacts, namely, on the downstream hydrological regime (i.e., alteration of high and low flow magnitude, frequency, and timing; see, e.g., Graf, 2006; Magilligan & Nislow, 2005; Wang et al., 2017), on geomorphology (i.e., sediment trapping, channel degradation or aggradation, and planform changes; see, e.g., Collier et al., 1996; Walker, 1985; Williams & Wolman, 1984), and on ecology (i.e., hydrologic and riparian disconnectivity; see, e.g., Nilsson & Berggren, 2000; Poff & Zimmerman, 2010; Pringle, 2003).

This paper focuses on the impacts of reservoirs on downstream flood peak discharges and particularly on the flood frequency curve. Because of the storage capacity of reservoirs, the postimpoundment flow regime is usually characterized by a reduction in the magnitude of maximum discharges and therefore of flood peak quantiles (Batalla et al., 2004; Graf, 2006; Magilligan & Nislow, 2001, 2005; Williams & Wolman, 1984). The amount of the downstream peak flow reduction is strongly dependent on the position of the reservoir in the catchment, its storage capacity, the operation rule, and the spatial configuration of multiple reservoirs (Ayalew et al., 2013, 2015, 2017).

In the scientific literature, the impacts of reservoirs on floods have been detected and quantified with (1) data-based studies and (2) continuous simulation analyses. Data-based studies look at the observed impacts of existing reservoirs. For example, even though some early investigations about deleterious effects of river structures had been conducted before (as reported in Graf, 2006), in the 1970s and 1980s, scientific studies started to take a census of major dams in the United States (Graf, 1999) and to document their downstream effects, analyzing predam and postdam discharge data (or, alternatively, pairs of upstream-unregulated and downstream-regulated reaches).

©2018. The Authors.
This is an open access article under the terms of the Creative Commons Attribution License, which permits use, distribution and reproduction in any medium, provided the original work is properly cited.

When analyzing many sites, the ratio between the reservoir storage capacity and the catchment area, or the mean annual runoff, has been identified as a useful index to quantify the magnitude of the potential flow alterations (Graf, 1999). In the context of river ecosystem research, Richter et al. (1996) introduced a method for the assessment of hydrological alteration consisting of 32 parameters (Indicators of Hydrological Alteration), organized into five groups, to statistically characterize hydrological variation within each year, which include floods. The method quantifies hydrological perturbations associated with anthropic activities, such as dam operations, by comparing the *preimpact* and *postimpact* indicators and their range of variability (Richter et al., 1996, 1998). This method, and its successive modification by Gao et al. (2009), has been applied in several local (e.g., Magilligan & Nislow, 2001; Zhang et al., 2014) and large-scale studies (e.g., Graf, 2006; Magilligan & Nislow, 2005). More recently, again, in the context of river ecosystem research, Ruhi et al. (2018) applied a wavelet analysis methodology in more than 100 sites across the United States to understand how the timing of river flows have changed due to a dam.

Similar data-based studies compare predam and postdam flood quantiles and hydrograph characteristics (Batalla et al., 2004; Singer, 2007) or changes of flood flows from regional regressions over different time periods (FitzHugh & Vogel, 2011; Pegg et al., 2003) or regional comparison of regulated and unregulated catchments (Assani et al., 2006). Recently, Wang et al. (2017) have used a reservoir index to investigate the effect of reservoirs on the mean and variation coefficient of the flood frequency curves in the Unites States and to explain their change in time.

The advantage of data-based approaches is that they are relatively simple and can be applied regionally on many catchments. They infer the *average* magnitude of the impacts of reservoirs on floods from many sites. They do so in a conceptual way, by using indexes that correlate with the peak reduction, but not in an integrated mechanistic way, that is, they do not explicitly quantify the relative effects of reservoir positioning, size, and operation rules on the flood frequency curve.

An alternative approach for the analysis of flow regulation impacts in catchments is the continuous simulation approach, consisting usually of a stochastic rainfall generator, a rainfall-runoff model, and a reservoir routing numerical model. For example, Bradley and Potter (1992) estimated flood frequency from continuous rainfall-runoff simulations for storage-regulated catchments, using a proposed runoff-volume-based approach. Hess and Inman (1994) studied the effects of urban flood-detention reservoirs on peak discharges and flood frequencies using an event-based rainfall-runoff model. More recent continuous simulation studies, for both real and hypothetical catchments, analyze the effects on discharge quantiles or peak discharge of spatially distributed small reservoirs and their spatial configuration (Ayalew et al., 2015, 2017; Montaldo et al., 2004) and the effects of reservoir capacity, operation rules, and the design of the release structures (Ayalew et al., 2013; Nehrke & Roesner, 2004). Their outcomes suggest that generally small distributed reservoirs significantly reduce flood magnitude, but their mitigation benefits are mainly local and diminish with the increase of the fraction of unregulated catchment area, contributing to peak discharge at the outlet.

The advantage of continuous simulation models is to explicitly account for the mechanisms determining the impacts of reservoirs on floods. In particular, the relative effects of reservoir positioning, size, and operation rules can be quantified. On the other hand, these modeling approaches are usually performed over few catchments and are not easily generalizable.

In order to combine the advantages of the data-based approach, that is, simplicity and applicability to many sites, and the advantages of the continuous simulation models, that is, to explicitly account for cause-effect mechanisms, we investigate in this paper the effects of reservoirs on peak discharge, based on a parsimonious Instantaneous Unit Hydrograph (IUH) method. In hydrology, the IUH, that is, the response hydrograph of the catchment to an instantaneous unit pulse of effective rain, is commonly used for flood design purposes. The geomorphological theory of the hydrological response (Geomorphological Instantaneous Unit Hydrograph), first proposed in a probabilistic framework by Rodríguez-Iturbe and Valdes (1979), links the hydrological response (IUH) to the catchment characteristics (i.e., geomorphology, hillslope, and channel flow velocity). Furthermore, the response hydrograph to an instantaneous unit pulse of effective rain (IUH) is conceptually equivalent to the probability density function (pdf) of travel times of a particle randomly precipitated on the catchment (Gupta et al., 1980). The underlying idea of the geomorphological theory is the derivation in closed form of the residence time distribution of a catchment, by taking into account the catchment morphology and the hydraulic characteristics of the flow along the channels (Rodriguez-Iturbe & Rinaldo, 1997). As an example, Di Lazzaro et al. (2016) developed a conceptual framework, based on the Geomorphological Instantaneous

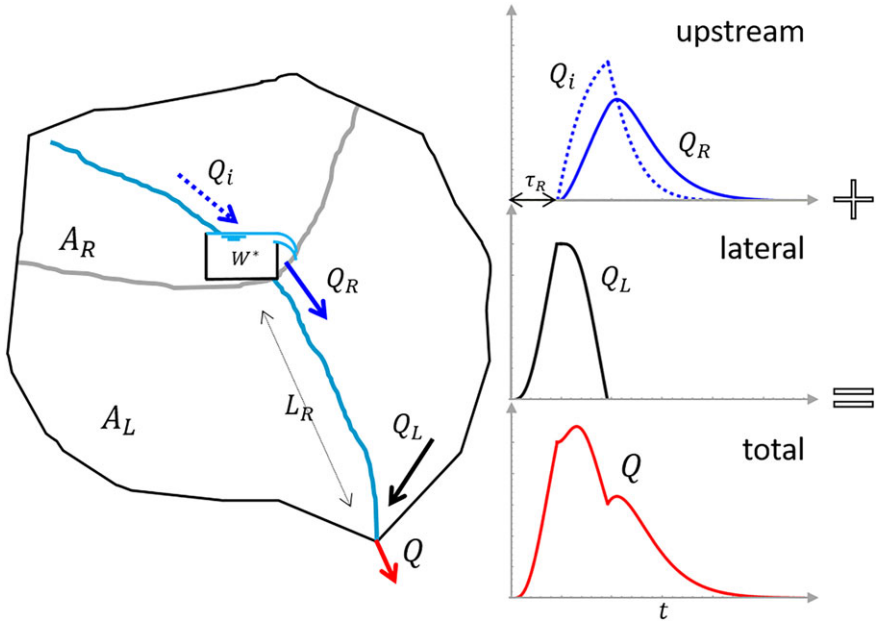

Figure 1. Sketch of the catchment where all the parameters relevant to the analyses are indicated (left); A_R is the upstream catchment area (L^2); A_L is the downstream catchment area (L^2); Q_i is the inflow to the reservoir (L^3T^{-1}), that is, the discharge from the upstream catchment; Q_R is the outflow from the reservoir (L^3T^{-1}); Q_L is the lateral inflow to the river (L^3T^{-1}), that is, the discharge from the downstream catchment; Q is the total river discharge (L^3T^{-1}); W^* is the volume of the reservoir (L^3); and τ_R is the temporal delay (T) due to the distance from the reservoir to the catchment outlet. The right panels depict how the contributions coming from the upstream catchment after the reservoir has been built (compared to that in natural condition) and the downstream catchment combines at the outlet.

Unit Hydrograph, to characterize the geomorphological and kinematic dispersive contribution to the hydrological response, particularly focusing on hillslope component; they obtain a general model for the derivation of the travel time distribution for idealized natural catchments.

In this paper we develop an IUH-based method that accounts for the presence of one reservoir in the catchment (section 2) and determines how the peak discharge quantile is attenuated as a function of few dimensionless numbers (section 3), which account for the position of the reservoir in the catchment, its volume, and its spillway. Note that among the simplifying assumptions, we do not consider the specific purpose of the reservoir, that is, its operation rules. The method is illustrated for idealized natural catchments and variable reservoir characteristics in section 4 and is used in a real-world case study in section 5. Section 6 summarizing the main findings of this work closes the paper.

2. Mathematical Framework

We consider a catchment of area A (L^2), where a reservoir for multiple uses including flood mitigation, or for flood mitigation only, is built along the mainstream river at a distance L_R (L) from the catchment outlet (as depicted in the sketch of Figure 1). The reservoir has a storage capacity W^* (L^3) and constitutes the outlet section of the upstream catchment of area A_R (L^2).

We use the classical theory of the IUH to model the hydrological response of the catchment to the excess rainfall. In natural conditions, before the reservoir construction, the flow discharge at the catchment outlet, Q (L^3T^{-1}), results from the convolution of the net rainfall, p (LT^{-1}), and the IUH, $u(\tau)$ (T^{-1}),

$$Q(t) = A \int_0^t p(t-\tau)\, u(\tau) \mathrm{d}\tau, \tag{1}$$

where τ (T) denotes travel time.

After the reservoir has been built, the flow discharge at the catchment outlet is the sum of (1) the discharge from the upstream catchment, Q_R, that is reduced with respect to its natural condition thanks to water storage,

and (2) the contribution of the intermediate/lateral catchment, Q_L, whose drainage area is $A_L = A - A_R$. Consistently with the IUH approach, the total discharge at the catchment outlet is given by $Q(t) = Q_R(t - \tau_R) + Q_L(t)$, where the upstream contribution Q_R is delayed to account for the time required for water to travel along the main channel at a constant channel velocity, v (L T^{-1}), that is $\tau_R = L_R/v$ (see Figure 1). The peak value of the upstream contribution, and consequently that of the total discharge, is reduced with respect to the natural condition; the relative reduction depends on the geomorphological and kinematic features of the catchment and of the reservoir characteristics, including its position along the mainstream.

2.1. Hydrological Response of the Upstream Catchment and Reservoir Routing

The inflow to the reservoir, denoted in the following as Q_i (Figure 1), can be computed by using equation (1), where A and u are substituted by A_R and u_R, respectively; u_R (T^{-1}) denotes the IUH of the upstream catchment.

Reservoir routing determines the outflow Q_R from a given inflow (Q_i) and known reservoir characteristics. It is computed by solving the continuity equation for storage in a reservoir, as

$$Q_i(t) - Q_R(t) = \begin{cases} \frac{dW(t)}{dt} & W(t) \le W^* \\ 0 & W(t) > W^*, \end{cases} \tag{2}$$

where W (L^3) is the volume of water stored in the reservoir. The two conditions in equation (2) account for the limited storage capacity of the reservoir, W^*, such that if the storage capacity is exceeded the difference between the outflow and the inflow becomes negligible or null.

2.2. Hydrological Response of the Lateral Catchment

The contribution coming from the lateral catchment (ii) is determined again as the convolution between the pertaining IUH and the net rainfall, as in equation (1). The IUH of the lateral catchment, denoted by u_L (T^{-1}), can be derived as the weighted difference between those of the whole ($u(\tau)$) and upstream ($u_R(\tau - \tau_R)$) catchments, as in the following

$$u_L(\tau) = \begin{cases} \frac{u(\tau) - A_R/A\, u_R(\tau - \tau_R)}{1 - A_R/A} & 0 \le A_R < A \\ 0 & A_R = A. \end{cases} \tag{3}$$

3. Peak Discharge Quantile Attenuation

We are interested in exploring the relative attenuation at the catchment outlet of peak discharge *quantiles*, that are peak discharges characterized by a given return period, T (T). To this aim, we consider a rectangular rainfall event of duration t_p (T) and intensity as extracted by an Intensity-Duration-Frequency (IDF) curve, $i(T, t) = a(T)t^{n-1}$ (L T^{-1}); the latter expression is that generally adopted in Italy and can be obtained by simplifying the general formula (see, e.g., Koutsoyiannis et al., 1998, equations 12 and 13). Further, we compute the net rainfall as a constant fraction of the total one, $p = \varphi\, i$, where φ is the runoff coefficient. Hence, the rainfall event with a given return period T is expressed by the following relationship

$$p(t) = \begin{cases} \varphi\, a(T)\, t_p^{n-1} & 0 < t \le t_p \\ 0 & \text{otherwise.} \end{cases} \tag{4}$$

Note that the above model assumes that the net rainfall is uniformly distributed over the catchment; this hypothesis is customary in design and risk assessment of hydraulic structures and coherent with the simplified IUH framework defined in the previous section.

To represent the hydrological response of the whole catchment to the net rainfall event in equation (4), we adopt the two-parameter gamma pdf as analytical model of the IUH. The gamma IUH, that is widely adopted in hydrological practice, was first derived by Nash (1957) on the basis of a linear reservoir cascade model and successively related to the geomorphological features of the catchment by Rosso (1984). The gamma (Nash) IUH is given by

$$u(\tau) = \begin{cases} \frac{e^{-\frac{m\tau}{\lambda}} \left(\frac{\lambda}{m}\right)^{-m} \tau^{m-1}}{\Gamma[m]} & \text{if } \tau > 0 \\ 0 & \text{otherwise,} \end{cases} \tag{5}$$

where λ (T) is the lag time, that is, the average of the travel time distribution (i.e., the IUH $u(\tau)$), and m is the number of linear reservoirs of the cascade. The latter parameter is directly related to the coefficient of

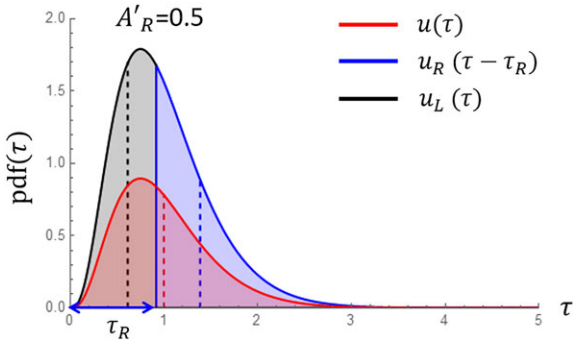

Figure 2. Instantaneous Unit Hydrograph of the upstream, $u_R(\tau - \tau_R)$, intermediate, $u_L(\tau)$, and whole catchments $u(\tau)$, for $m = 4$ and $A'_R = 0.5$. Note that the Instantaneous Unit Hydrograph of the upstream catchment is delayed of the temporal distance from the reservoir to the catchment outlet, τ_R. Vertical-dashed lines indicate the corresponding lag times. pdf = probability density function.

variation (CV) of the travel time distribution, $m = 1/CV^2$; according to the variability of the geomorphological (and kinematic) features in a natural catchment, m assumes values in the range [2, 8] (Rosso, 1984). In spite of its simplicity compared to other models, such as that proposed by (Di Lazzaro et al., 2016), the Nash IUH allows to take into account the most important parameters controlling the hydrological response of natural catchments in presence of reservoirs (as discussed in the case study proposed in section 5).

Following equation (1), the flow discharge at the catchment outlet in natural conditions is given by the following relationships, written in dimensionless variables

$$\frac{Q'(t')}{(t'_p)^{n-1}} = \begin{cases} \Phi(t') & t' \le t'_p \\ \Phi(t') - \Phi(t' - t'_p) & t' > t'_p, \end{cases} \tag{6}$$

where the function Φ is defined based on the incomplete gamma function Γ as

$$\Phi(t') = 1 - \frac{\Gamma(m, m\,t')}{\Gamma(m)}, \tag{7}$$

and $Q' = Q/(\varphi\, a(T)\, \lambda^{n-1} A)$, $t' = t/\lambda$, and $t'_p = t_p/\lambda$. Since $Q(t)$ depends on rainfall duration through the IDF curve, we search for the t'_p value that maximizes the peak discharge quantile, $\theta = \text{argmax}\, Q'_{\max}(t'_p)$, thus finding the most critical condition for each return period (i.e., design storm method; see, e.g., Pilgrim & Cordery, 1993, page 9.13).

For simplicity and without loss of generality, we suppose that u_R is derived from u by lower truncating the pdf at the temporal distance of the reservoir from the catchment outlet, τ_R, as in the following

$$u_R(\tau) = \frac{1}{A_R}\, u(\tau | \tau > \tau_R), \tag{8}$$

where the truncated distribution is normalized to its mass, A_R, to let u_R be a proper distribution (integrating to one; an example is depicted in Figure 2). In other words, we suppose that the upstream catchment is bounded downstream by the τ_R isoline of travel time. Note that this simplifying assumption does not affect, in essence, the results of our analyses, as it will be demonstrated in the real-world case study presented in section 5. Also note that this assumption is consistent with the generalized case of having more reservoirs located in the headwater part of a catchment, approximately at the same distance to the outlet. To solve reservoir routing in equation (2), we assume a linear relationship between the outflow and the volume of stored water (see section 5 for a discussion on the implications of this assumption), that is, $Q_R = W/K$; K (T) is the storage coefficient that determines the attenuation of the outflow with respect to the inflow, being a measure of the ratio between the storage area and the spillway dimensions; hence, K does not depend on the volume W or on the storage capacity W^*. Thanks to this linearity assumption, equation (2) can be analytically solved; starting from the initial condition of empty reservoir, $W(0) = 0$, its solution is given by

$$Q_R(t) = \begin{cases} \int_0^t Q_i(t-\tau)\, f_R(\tau) \mathrm{d}\tau & Q_R(t) \le W^*/K \\ Q_i(t) & Q_R(t) > W^*/K, \end{cases} \tag{9}$$

where $f_R(\tau) = \frac{1}{k} e^{-\frac{\tau}{k}}$ (T^{-1}). Hence, the outflow for the reservoir can be estimated by first determining the discharge flowing into the reservoir Q_i, which requires to solve the convolution between the net rainfall (equation (4)) and the upstream IUH (equation (8)) and, second, by solving the convolution between Q_i and the reservoir function f_R (equation (9)); the analytical solution of the convolution integral in the first line of equation (9) is provided below

$$\frac{Q'_R(t')}{(t'_p)^{n-1}} = \left(1 - \frac{1}{K'\,m}\right)^{-m} \begin{cases} \left(1 - \frac{1}{K'\,m}\right)^m \left[\Phi(t' + \tau'_R) - \Phi(\tau'_R)\right] + \\ e^{-\frac{t'+\tau'_R}{K'}} \cdot \left[\Phi\left(\left(1 - \frac{1}{K'\,m}\right)\tau'_R\right) - \Phi\left(\left(1 - \frac{1}{K'\,m}\right)(t' + \tau'_R)\right)\right] & t' \le t'_p \\ \left(1 - \frac{1}{K'\,m}\right)^m \left[\Phi(t' + \tau'_R) - \Phi(t' - t'_p + \tau'_R)\right] + \\ e^{-\frac{t'+\tau'_R}{K'}} \cdot \left[\Phi\left(\left(1 - \frac{1}{K'm}\right)\tau'_R\right) - \Phi\left(\left(1 - \frac{1}{K'\,m}\right)(t' + \tau'_R)\right)\right] + \\ -e^{-\frac{t'-t'_p+\tau'_R}{K'}} \cdot \left[\Phi\left(\left(1 - \frac{1}{K'm}\right)\tau'_R\right) - \Phi\left(\left(1 - \frac{1}{K'\,m}\right)(t' - t'_p + \tau'_R)\right)\right] & t' > t'_p, \end{cases} \tag{10}$$

where Φ is given in equation (7) and $\tau'_R = \tau_R/\lambda$ (i.e., the dimensionless temporal distance of the reservoir from the catchment outlet). When the storage capacity is a limiting factor, we have $Q'_R(t') = Q'_i(t')$ according to the second line of equation (9).

The contribution coming from the lateral catchment (Q'_L) results again from the convolution of the net rainfall $p(t)$ (given by equation (4)) and the lateral IUH, $u_L(\tau)$, as expressed by equation (1) but with $A = A_L$ and $u = u_L$. The lateral IUH u_L is expressed by (equation (3)) with u given by equation (5) and u_R as in equation (8). Thus, we obtain

$$\frac{Q'_L(t')}{(t'_p)^{n-1}} = \begin{cases} \Phi(t') & t' \le t'_p,\ t' < \tau'_R \\ \Phi(t') - \Phi(t' - t'_p) & t' > t'_p,\ t' < \tau'_R \\ \Phi(\tau'_R) & t' \le t'_p,\ t' \ge \tau'_R \\ \Phi(\tau'_R) - \Phi(t' - t'_p) & t' > t'_p,\ t' \ge \tau'_R,\ t' < (t'_p + \tau'_R). \end{cases} \tag{11}$$

Finally, the total discharge at the catchment outlet results from the sum of the above equations (10) and (11), that is, $Q(t) = Q_R(t - \tau_R) + Q_L(t)$. We focus again on the rainfall duration that maximizes the peak discharge quantile; after the reservoir construction, the maximum peak discharge quantile is obtained for a rainfall duration, denoted in the following as θ_R, generally different from that pertaining in the natural (before the reservoir construction) case, θ.

Following equations (6), (10), and (11), the relative attenuation of peak discharge quantile with respect to natural conditions is a function of the following dimensionless parameters:

- $A'_R = A_R/A$, which measures the ratio of the whole catchment area that is controlled by the reservoir; thanks to the simplifying assumption on the IUH shape of the upstream catchment (u_R as in equation (8)), this parameter fully determines the distance of the reservoir from the outlet;
- $K' = K/\lambda$, which represents the delay in the outflow due to the storage in the reservoir with respect to the average travel time of the whole catchment (lag time);
- $W^{*\prime} = \frac{W^*}{K\ \varphi\ a(T)\ \lambda^{n-1}\ A}$, which is the relative storage capacity with respect to the whole catchment dimension, hydrological (rainfall) load, and reservoir characteristics.

4. Results

In this section we illustrate and discuss how the relative attenuation of peak discharge quantile with respect to natural conditions is ruled by the dimensionless controlling parameters, A'_R, K', and $W^{*\prime}$. We assume $m = 4$, which means that the coefficient of variation of the travel time distribution of the catchment is $CV = 0.5$; further, we assume the slope of the IDF curve $n = 0.3$, which characterizes, for example, the average climate of central Italy. As stated in the previous section we search for the critical conditions; hence, we focus on the dimensionless rainfall duration, θ or θ_R, that maximizes the natural and the controlled discharge, respectively. Figure 2 compares the IUH of the whole catchment to those of the upstream and lateral catchments (where vertical-dashed lines are the corresponding lag times), according to their definitions provided in sections 2.1 and 2.2, when assuming $A'_R = 0.5$; note that the IUH of the upstream catchment is delayed of τ_R for the sake of clarity. The corresponding discharges in natural conditions for a critical rainfall event, that is, with duration θ that maximizes the total discharge, are depicted in Figure 3a; the inset in Figure 3a depicts how peak discharge quantile ($Q'_{\max}$) behaves as function of the rainfall duration, t'_p. The critical rainfall event is characterized by a duration ($t'_p = t_p/\lambda$) slightly smaller than the lag time λ, that is, $\theta < 1$ (see Figure 1).

We consider a reservoir with $K' = 0.5$ and a very large storage capacity, such that the second condition in equation (9) is never met. Discharges after reservoir are depicted in Figure 3b. Both the upstream and lateral hydrographs change with respect to the natural condition (Figure 3a) due to the different critical rainfall event; the upstream contribution is also affected by the storage in the reservoir. As expected, the peak discharge quantile is attenuated. It is interesting to note that, in this specific case, the peak discharge quantile after reservoir is due only to the uncontrolled lateral contribution downstream the reservoir (i.e., the maximum value of the total discharge, red line, is that of the lateral one, black line). Hence, the critical rainfall event for the whole catchment is that critical for the lateral catchment; since the latter has a smaller area than the total one ($A_L = A - A_R$) and smaller lag time (see Figure 2), the rainfall duration that maximizes the total discharge is smaller than in natural conditions, $\theta_R < \theta$ (as shown in the inset of Figure 3b).

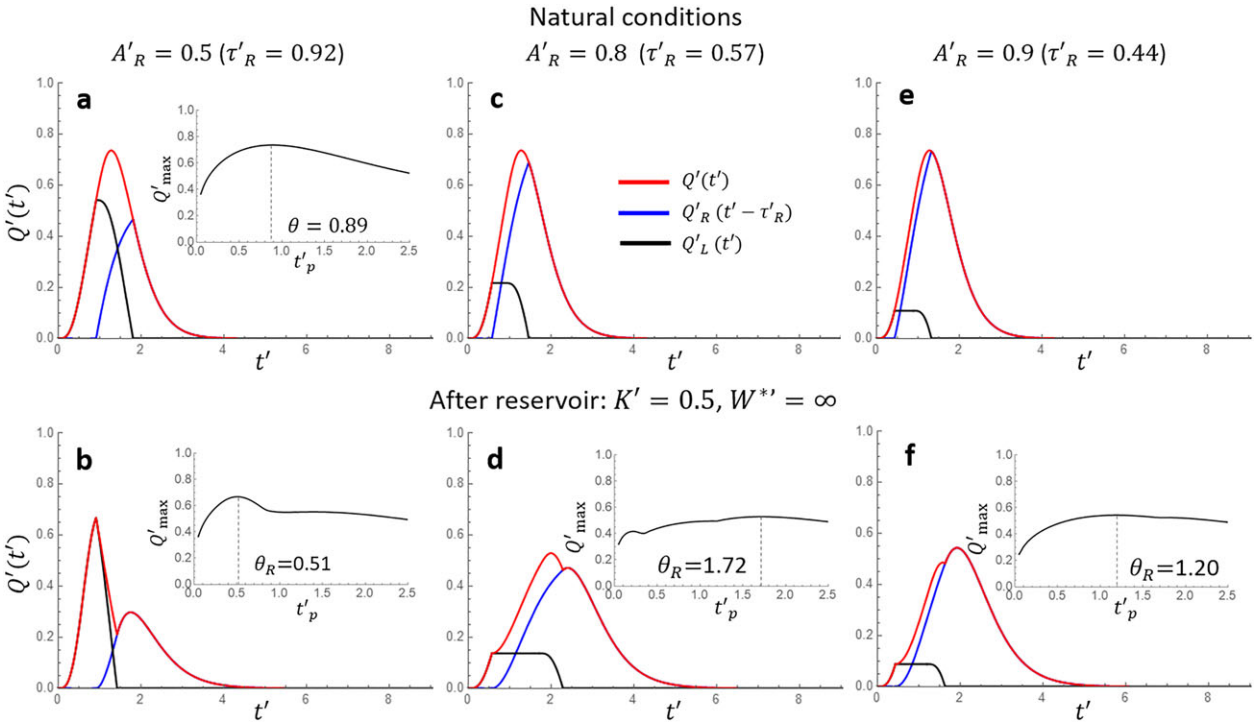

Figure 3. Discharge quantile of the upstream, $Q'_R(t'-\tau'_R)$, intermediate, $Q'_L(t')$, and whole catchments, $Q'(t')$, obtained for $m = 4$, $n = 0.3$, and $A'_R = \{0.5, 0.8, 0.9\}$ (left, middle, and right panels, respectively) and $t'_p = \theta$ (i.e., the critical rainfall event duration); (a), (c), and (e) show how the contributes of the upstream and lateral catchments combine in natural conditions, while the (b), (d), and (f) depict the combination of the contributes after a reservoir with very large storage capacity (W^*) and storage coefficient $K' = 0.5$ has been built. The inset in each panel depicts how peak discharge quantile behaves as function of rainfall duration t'_p; note that under natural conditions, the critical rainfall duration, θ, is the same for each potential position of the reservoir, that is, for each potential value of A'_R.

For larger A'_R, which means a reservoir position closer to the catchment outlet, the combination of the upstream and lateral contributions might change. Results for $A'_R = 0.8$ are shown in Figures 3c and 3d. In the natural condition (Figure 3c), the two hydrographs of the upstream and intermediate catchments combine in a different way and sum up to the total discharge at the catchment outlet, that is obviously unchanged with respect to Figure 3a (as it is unchanged the rainfall duration that maximizes the discharge, as shown in the inset of Figure 3a). The effect of reservoir attenuation due to its position ($A'_R = 0.8$) is shown in Figure 3d; in this case, the peak discharge quantile is mainly controlled by the upstream contribution (blue line), that is much larger with respect to the lateral one. However, the lateral one still plays a role; indeed, the peak value of total discharge (red line) does not coincide with that of the upstream controlled catchment (blue line). The critical rainfall event has a rainfall duration θ_R that is much larger than in the previous case, $\theta_R > \theta$, as clearly depicted in the inset of Figure 3d.

If the controlled area continues to increase (Figures 3e and 3f), the peak discharge quantile becomes totally controlled by the upstream contribution and the critical rainfall event is that of the upstream catchment. The critical rainfall duration θ_R is again slightly smaller than the upstream lag time; note that the latter is delayed due to the temporal distance of the reservoir from the outlet (τ_R, as depicted in Figure 2) and the storage effect (K').

Figure 4 summarizes results obtained when storage is not a limiting condition (large values of $W^{*\prime}$), with different storage coefficients K' ranging between 0.1 and 20, as function of the controlled area A'_R. Results are depicted in terms of the ratio between the peak discharge quantiles after reservoir and in natural conditions, that is the relative attenuation $R_Q = \frac{Q'_{\max}|_{nat.} - Q'_{\max}|_{res.}}{Q'_{\max}|_{nat.}}$ (Figure 4a), and of the critical rainfall duration, θ_R (Figure 4b).

Figure 4 shows that, for every value of the storage coefficient K', there are three ranges of variability of the ratio R_Q and the critical duration θ_R that correspond to the cases illustrated in Figure 3. The first range of positions (those farther from the catchment outlet) is characterized by the fact that peak discharge is ruled only by the lateral contribution. In this range, the ratio R_Q and the critical duration θ_R (Figure 4b) decrease when increasing

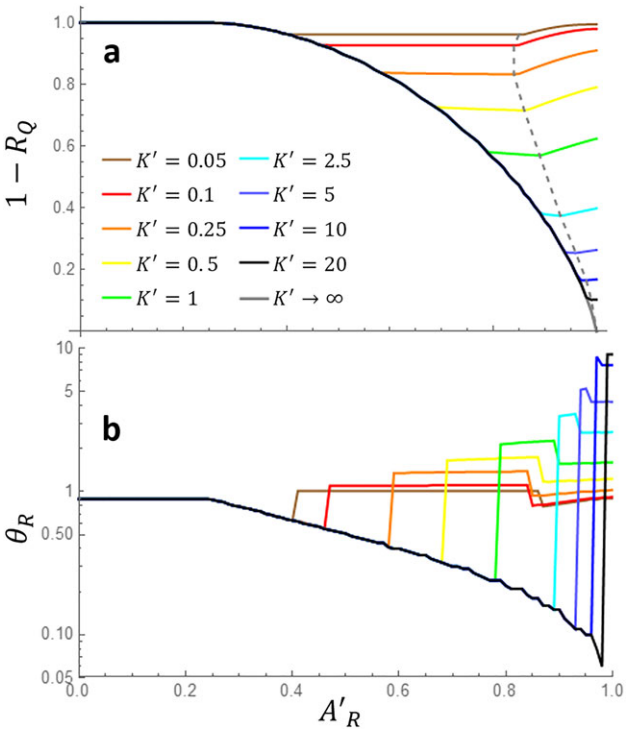

Figure 4. (a) Relative attenuation of the flood quantile, $1 - R_Q$, and (b) rainfall duration that maximizes discharge after reservoir construction, θ_R, as functions of the reservoir position; we recall that reservoir position is measured in terms of the catchment area upstream the reservoir, A'_R. We assumed $m = 4$, $n = 0.3$, and several values of the storage coefficient, K', for the case of infinite storage capacity $W^{*\prime}$. The gray-dashed line in (a) joins the optimal positions of the reservoir (A'_R) for all the value of the storage coefficient K' considered in the analysis.

A'_R as a consequence of the reduction of the lateral catchment area. The extension of this range depends on the storage coefficient and is larger in the case of very high K' values. When increasing further A'_R, we can observe that the ratio R_Q continues to decrease but at a smaller rate; in this second range, the peak discharge starts to be ruled by the upstream contribution, even if the lateral one still plays a role. The transition between the first and the second range of variability is characterized by a positive jump in the rainfall duration that maximizes the peak discharge, as depicted in Figure 4b. Larger jumps in θ_R are associated with high values of the storage coefficient K', that is, larger delay in the response time of the upstream catchment. Further, in this second range the critical duration increases with A'_R (even slightly) thanks to the increases of the upstream catchment area. Finally, there is a position where R_Q reaches its maximum value; this position represents the transition from the second range to the third one, where the peak is ruled only by the upstream contribution. The optimum position of the reservoir as function of the storage coefficient is represented by the gray-dashed line in Figure 4a. The transition is again characterized by a jump in θ_R, yet negative in this case. Hence, by varying A'_R, this critical duration shifts abruptly at the positions in which the flood peak is dominated by the downstream catchment only, by both parts of the catchment, and by the upstream catchment only; this is because our model relates the relevant extreme storm duration to the catchment response time and the latter to catchment area (see, e.g., Gaál et al., 2012).

While the optimum lies at the transition between the second and the third ranges, every position (A'_R) within the second range could be considered for design purposes, since both attenuation (Figure 4a) and critical rainfall duration (Figure 4b) are almost constant. For distances between reservoir and catchment outlet larger than this range, the flood peak is dominated by the discharge from the catchment downstream the reservoir, and the attenuation is not optimal because this contribution is large. For shorter distances, instead, the peak is ruled only by the discharge from the upstream catchment but the attenuation is not optimal because the advantage of separating the two peaks from the upstream and downstream catchments is lost. The extension of the optimal range is ruled by the storage coefficient, being large in the case of small K' values; however, it can be significantly reduced if the storage capacity $W^{*\prime}$ is a limiting factor, as discussed later on.

Further, it is important to stress that, thanks to the linearity of the system, the attenuation of peak quantile and the optimum position do not depend on the quantile return period, T, which rules the IDF curves only by means of the term $a(T)$ (as in equation (4)). This implies that the curves depicted in Figure 4 provide a quantification of the relative flood attenuation for any return period value. Conversely, the curves are affected by the slope n of the IDF curve that determines how much rainfall intensity changes with the duration t_p; following equations (10) and (11), the larger is n, the smaller is the relative attenuation R_Q due to the modest relative increase of the critical rainfall duration in the optimum range with respect to natural conditions. Figure 5 shows the relative attenuation $1 - R_Q$ (Figure 5a) and critical rainfall duration (Figure 5b) when assuming $K' = 0.5$ and for several values of n in the interval between 0.2 and 0.6; values of n in between 0.2 and 0.4 are typical in central Italy, while larger values up to 0.6 can be found in the Alps regions (i.e., extreme rainfall intensity varies more strongly with duration in central Italy than in the Alps) as a result of the VAPI Project (Rossi & Villani, 1994). The figure also depicts the effect on quantile attenuation of the parameter m; we recall that m controls the coefficient of variation of the travel time distribution according to the variability of the geomorphological features in a natural catchment, that is, the distribution of the hillslope and channel lengths and of the kinematic parameters determining the velocity of catchment response. Generally speaking, small values of m pertain to catchments where the contributing area is close to the catchment outlet. Within the range of variability as provided by Rosso (1984), which approximately corresponds in term of coefficient of variation to the range $[0.35 - 0.70]$, the value of m does not influence significantly the reservoir effect on flood quantiles.

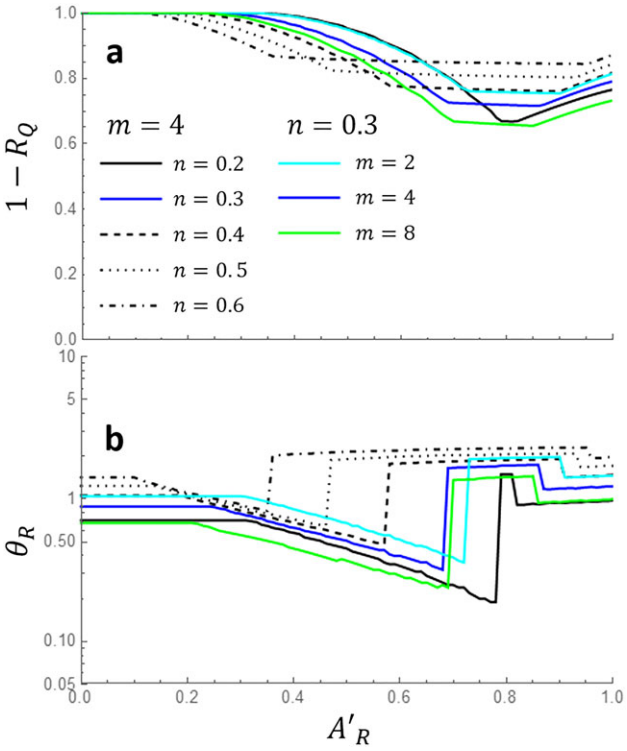

Figure 5. (a) Relative attenuation of the flood quantile, $1 - R_Q$, and (b) rainfall duration that maximizes discharge after reservoir construction, θ_R, as functions of the reservoir position A'_R, for several values of the Intensity-Duration-Frequency slope n, when assuming the geomorphological parameter $m = 4$, and for $n = 0.3$ (as in Figure 4), when assuming $m = 2$ or $m = 8$; those values are the limits of the range of variability of m according to Rosso (1984); for all the combination of n and m we considered $K' = 0.5$.

When $W^{*\prime}$ becomes a limiting factor, the behavior depicted in Figure 4 becomes less pronounced. Figure 6 shows the relative attenuation $(1 - R_Q)$ as function of the upstream catchment area A_R for several values of $W^{*\prime}$; note that $W^{*\prime}$ depends on the storage coefficient K. The smaller is the storage capacity, the smaller is the relative attenuation R_Q that obviously tends to zero (no attenuation) when $W^{*\prime} \to 0$. The limited storage capacity also affects the extension of the three ranges of A'_R values: the extension of the first two ranges reduces, especially that of the second one that tends to vanish in favor of the third range, where the upstream contribution determines the peak discharge value. The attenuation effect depicted in Figure 6 may also represent the condition of a large reservoir whose storage capacity for flood attenuation is partially filled when the critical rainfall event occurs. Note that although the peak attenuation as depicted in Figure 4 is valid for any return period value T, the curves depicted in Figure 6 are affected by T through the dimensionless parameter $W^{*\prime}$, such that $W^{*\prime}$ measure the storage capacity with respect to a given return period hydrological load.

In summary, there is an optimum in the reservoir position that is close to the catchment outlet for large storage (i.e., very large values of K' and $W^{*\prime}$); the storage effect allows to obtain peak discharge quantiles that are smaller (even slightly) than the only contribution of the lateral catchment (first range).

5. Case Studies: Paglia and Chiani Rivers (Italy)

We explore now the influence of the IUH shape on the optimum in the reservoir position by considering two study cases, namely, the Paglia and Chiani rivers (Italy). Our main scope here is to understand to what extent the simplifying assumption related to catchment morphology adopted in the framework might limit the model application to real-world case studies. Further, we investigate the role of the linear reservoir assumption on the attenuation of flood quantiles by comparing results for linear and nonlinear reservoirs. We remark that we do not perform here any model assessment based on streamflow data before and after the construction of a reservoir, which, however, necessitates long records of data, reservoir management rule, model calibration, and so on that will be addressed in future works. Conversely, we consider several positions along the main stream for a hypothetical reservoir with variable characteristics, storage coefficient, and capacity.

The Chiani River is the main tributary of the Paglia River (see Figure 7a); at their confluence, the corresponding drainage areas are 780 and 450 km^2, respectively, while their main channel lengths are both about 60 km. The two catchments differ in terms of their geomorphological features; while the Paglia catchment shows a classical *mountain-plain* pattern, with hillslopes that generally become flatter and longer as we move close to the catchment outlet, the Chiani River depicts a *plateau-gorge* pattern, where the flatter and longer hillslopes are located in the upper or middle part of the catchment. The contrasting geomorphological property of the two catchments, which is illustrated in Figure 7b in terms of the spatial distribution of the hillslope-to-channel lengths (L_h [L]), results in two different IUH shapes (see Figure 7c). In the following we recall the main points of the procedure used to derive the geomorphological IUH; the reader is referred to Di Lazzaro (2009) for further details.

The geomorphological IUH (i.e., the rescaled width function) is derived based on a two step procedure: first, the hydrological pathways are identified and rearranged to obtain the geomorphological width function; second, hillslopes and channels are topologically separated to compute hillslope-to-channel and channel distances and the corresponding travel times. Drainage paths are derived by applying a conventional terrain analysis to each pixel of a raster cell of a Digital Elevation Model with grid spacing of 20×20 m. To determine whether a site belongs or not to the channelized part of the catchment, we adopt the procedure based on the total upstream contributing area ($\mathcal{A}$ [L^2]) and the local slope of the elevation field (s), through the threshold

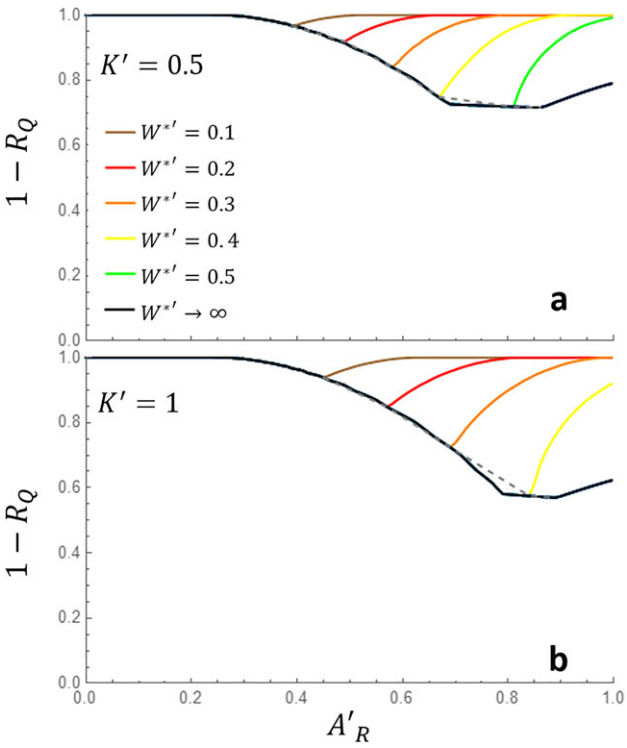

Figure 6. Relative attenuation, $1 - R_Q$, as a function of the reservoir position A'_R for $m = 4$, $n = 0.3$, and several values of the storage capacity, $W^{*\prime}$: (a) $K' = 0.5$ and (b) $K' = 1$. The gray-dashed line joins the optimal position of the reservoir for all the values of the storage capacity $W^{*\prime}$ considered in the analysis.

slope-area criterion $As^2 > \chi$ where we assumed $\chi = 5,000$ m^2. Once hillslope-to-channel (L_h [L]) and channel (L_c [L]) distances are estimated, the corresponding travel time is derived for each site as $\tau = L_c/u_c + L_h/u_h$, where u_c and u_h are the channel and hillslope velocities (LT^{-1}). Finally, the geomorphological IUH is derived as the empirical probability distributions of travel times (τ). The kinematic parameters u_c and u_h rule the geomorphological IHU model; in this study their values are fixed spatially uniform and equal to $u_c = 0.03$ m/s and $u_h = 1.55$ m/s for both the study catchments (Di Lazzaro, 2009), such that the difference between the IUH depicted in Figure 7c only depends on the lengths distribution.

Although the Paglia River has a much larger contributing area with respect to the Chiani River, the two catchments has a similar average lag time (Figure 7c). Flow concentration at the Paglia outlet occurs relatively more rapidly than at the Chiani outlet due to the superposition of the contributes coming from the upper part of the catchment with those coming from the areas close to the outlet (where larger hillslopes are); this is a consequence of the geomorphological pattern and of the different hillslope and channel velocities. Further, there is a nonnegligible part of the catchment located close to the outlet that responds very quickly; this yields a small value of the critical rainfall duration with respect to that pertaining to the Chiani river under natural conditions.

For both the catchments, we explore several possible positions for the reservoir along the main river (which are represented as white triangles in Figure 7b); those positions are arbitrarily chosen in order to explore the whole range of areas $0 \le A_R \le A$ (as in the synthetic case described above), without taking into account the practical feasibility, which goes far beyond the scope of this work. Rectangular rainfall events are extracted by the average IDF curves that characterize the rainfall regimes in the two catchments; the slope of the IDF curves is $n = 0.25$.

Reservoir routing is determined by solving the mass balance as in equation (2), where we relaxed the approximation of linear reservoir adopted in previous sections; we do introduce this extension in order to evaluate how does the linearity assumption made in the previous sections affect the results. Thus, we introduce here the typical spillway relationship, $Q_R = CBh^{3/2}$, where C is the spillway coefficient (whose numerical value depends on the type of spillway), B is the spillway length, and h is the water level in the reservoir above the spillway crest. Here we assume a broad-crested spillway, such that $C \simeq 1.77$ (m$^{1/2}$/s). As the volume of water stored in the reservoir W is related to the outflow Q_R through the reservoir area Ω, equation (2) becomes

$$Q'_i(t) - Q'_R(t) = \begin{cases} \frac{2}{3}\kappa' \frac{dQ'_R(t)}{dt} Q'^{-1/3}_R & W'(t) \le W^{*\prime} \\ 0 & W'(t) > W^{*\prime}. \end{cases} \tag{12}$$

When using the above dimensionless equation to determine the total discharge $Q'(t) = Q'_R(t' - \tau_R) + Q'_L(t')$, the relative attenuation of peak discharge quantile with respect to natural conditions is a function of A'_R and the following dimensionless parameters:

- $\kappa' = \kappa/\lambda = [\Omega/((CB)^{2/3}(\varphi\, a(T)\, \lambda^{n-1}A)^{1/3})]/\lambda$, which represents the delay in the outflow due to the storage in the reservoir with respect to the average travel time of the whole catchment (lag time);
- $W^{*\prime} = CB(W^*/\Omega)^{3/2}/(\varphi\, a(T)\, \lambda^{n-1}\, A)$, which is the relative storage capacity with respect to the whole catchment dimension, hydrological (rainfall) load, and reservoir characteristics.

Note that compared to the synthetic model illustrated in previous sections, the relative attenuation in this case depends on return period T through κ' also in the case of unlimited storage capacity (very large values of $W^{*\prime}$).

Figures 8a and 8b summarizes results obtained for both the Paglia and Chiani rivers when considering $T = 100$ years, very large storage (large values of $W^{*\prime}$), and different storage coefficients $\kappa' = \{0.1, 1, 10\}$, as

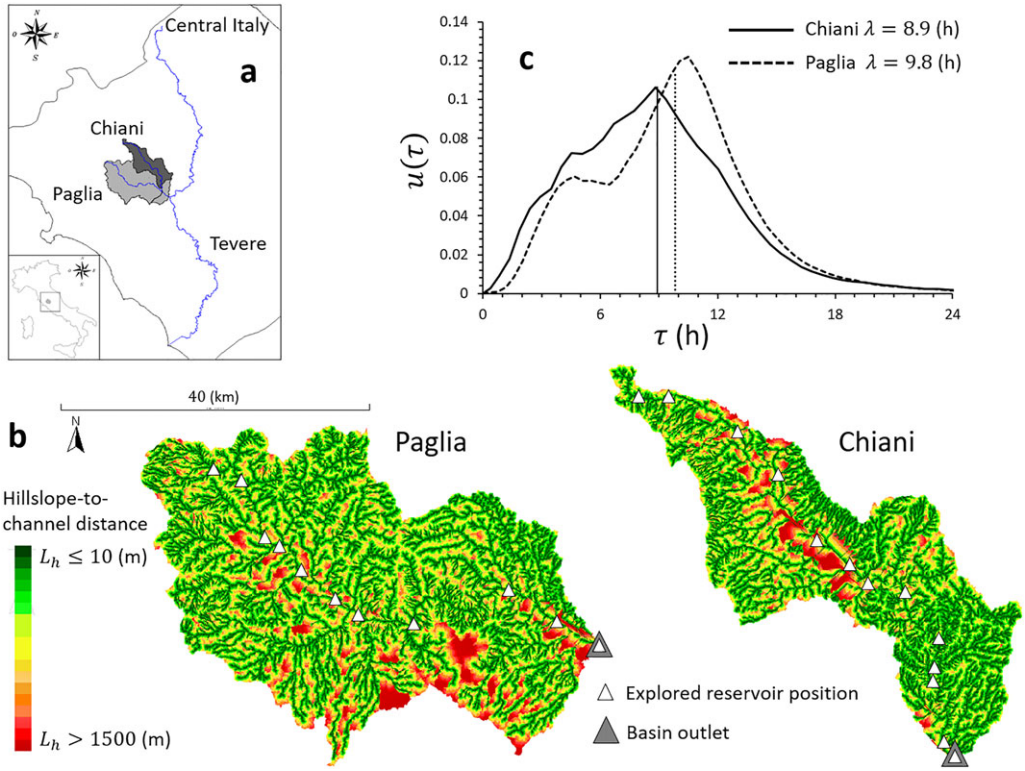

Figure 7. Paglia and Chiani rivers catchments: (a) location of the two catchments in Central Italy; (b) spatial distribution of hillslope-to-channel length, L_h, for each catchment separately (Paglia on the left and Chiani on the right). (c) For both Paglia and Chiani rivers, we report the geomorphological Instantaneous Unit Hydrograph at the catchment outlets, $u(\tau)$, where the average of the travel time distribution, that is, the lag time λ, is reported for each of the catchments.

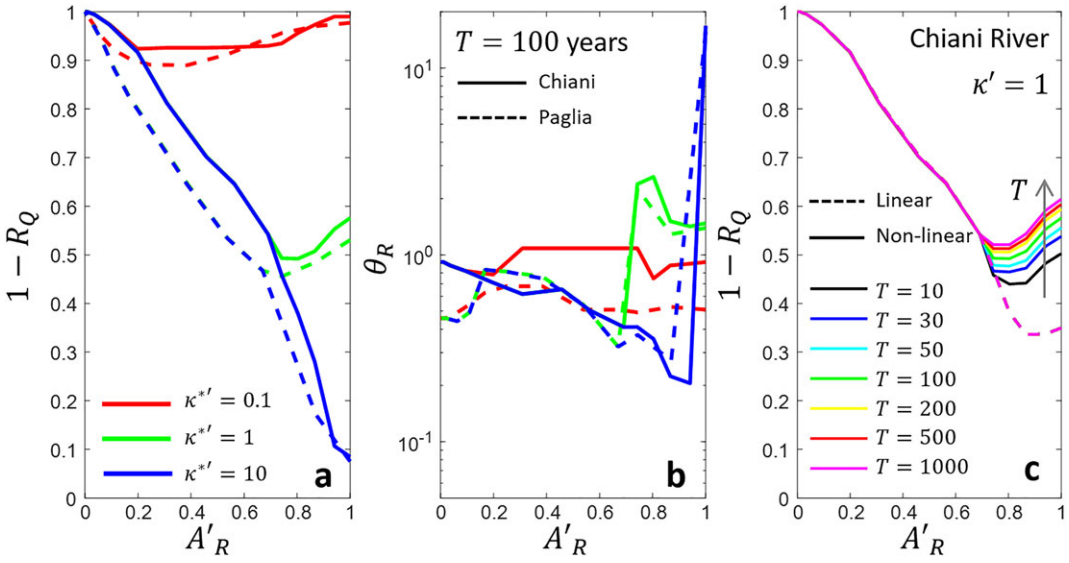

Figure 8. (a) Relative attenuation of flood quantile, $1 - R_Q$, and (b) critical rainfall duration after reservoir construction, θ_R, as functions of the reservoir position, A'_R, for Paglia (dashed lines) and Chiani catchments (solid lines) and three different values of the storage coefficient, $\kappa' = \{0.1, 1, 10\}$. (c) Relative attenuation of flood quantile, $1 - R_Q$, for the Chiani catchment, when assuming $\kappa' = 1$ and several values of the return period ranging between $T = 10$ and $T = 1,000$ years. Relative attenuation is computed by considering both a linear (equation (2), dashed lines) and a nonlinear reservoir (equation (12), solid lines). Note that in the case of linear reservoir, the attenuation of flood quantile is not affected by the return period T (curves for different T collapse on a single curve).

function of the controlled area A'_R. Results are depicted in terms of the ratio between the peak discharge quantiles after reservoir and in natural conditions, that is the relative attenuation $1 - R_Q$ (Figure 8a), and of the critical rainfall duration, θ_R (Figure 8b). Results are very similar to those depicted in Figure 4: there is an optimum in the reservoir position that is close to the catchment outlet for large storage (very large values of k'), that is determined by the relative increase of critical rainfall duration with respect to natural conditions. This confirms that the simplifying assumption of deriving u_R from u by lower truncating the pdf at the temporal distance of the reservoir from the catchment outlet τ_R used for the idealized catchment in section 3 does not affect significantly the general behavior of quantile attenuation due to reservoirs. Further, we can notice that the relative attenuation is stronger for the Paglia River, where the minimum flood quantile is obtained for critical rainfall duration relatively much larger than that pertaining to the natural conditions.

As previously mentioned, while results obtained for an idealized catchment illustrated in previous sections (Figure 4) do not depend on the return period T, those shown in Figure 8 depend on T through κ', due to the nonlinearity of reservoir routing in equation (12). The effect of return period on the relative attenuation of the Chiani River is depicted in Figure 8c. Figure 8c shows the quantile attenuation for several values of return period ranging from $T = 10$ and $T = 1,000$ years for $\kappa' = 1$ and compares it to those obtained for the same return period values by using a linear reservoir routing, as in equation (2); the comparison is performed by preserving storage dimensions (the reservoir area Ω and the spillway length B). Attenuation R_Q is smaller ($1 - R_Q$ is higher) for a nonlinear reservoir than a linear one, since the discharge from the spillway grows up more rapidly with storage water level for a typical spillway than in the linear case. Note that we assumed in the linear case $K = \Omega/(CB)$ with the same value for the spillway coefficient C as in the nonlinear case to facilitate the comparison. R_Q reduces with T (we have ~10% variation for $T \in [10 - 1,000]$). Also, the optimal position is slightly varying with T, moving from downstream to upstream of ~5%.

6. Discussion and Conclusions

A parsimonious IUH-based method is proposed to quantify the attenuation of flood peak discharges in rivers due to reservoirs. Three main system characteristics are shown to control this attenuation and are quantified through dimensionless numbers: (1) the reservoir position along the river channel, quantified by A'_R, the ratio of the catchment area above the reservoir and the total area; (2) the spillway dimensions, quantified by K', the ratio between the reservoir storage coefficient and the catchment average response time; and (3) the storage capacity, quantified by $W^{*\prime}$, the ratio of the storage volume and the volume of water expected from an extreme precipitation associated to a given return period (i.e., the hydrological load) that can be released by the reservoir spillway. The three dimensionless numbers are derived analytically for an idealized catchment, and the implications of assumptions about catchment morphology and the linear reservoir release are investigated in two real catchments where the IUHs are derived based on their geomorphological and kinematic features, by allowing a nonlinear spillway relationship.

The following main conclusions can be stated:

- The attenuation of the flood peaks is due to the retention of the water in the reservoir (i.e., the same volume of water is released within a larger time, thus smoothing the wave) and to the separation between the peaks produced in the catchments upstream and downstream the reservoir (because of the delay due to the retention in the reservoir).
- The amount of flood peak attenuation increases for increasing storage coefficient K', which determines the retention of water in the reservoir, and reservoir capacity $W^{*\prime}$, as would be expected; actually, $W^{*\prime}$ is analogous to the reservoir indexes used in the literature (see, e.g., Graf, 1999; Wang et al., 2017). These dependencies on $W^{*\prime}$ and K' vary as a function of the relative position A'_R.
- An optimal position exists for the reservoir that allows to maximize flood quantile attenuation at the catchment outlet, with respect to the natural conditions (those without the reservoir); this optimal position (i.e., the optimal A'_R) is, in general, not at the catchment outlet, but is closer to it for larger storage coefficient K' and capacity $W^{*\prime}$.
- Interestingly, our analysis shows that, for large reservoir capacity and relatively small spillways, a range of nearly optimal positions exists. For small relative reservoir volumes (i.e., for small $W^{*\prime}$), the range of nearly optimal positions collapses to a single location (i.e., the optimal A'_R). The size of this range also strongly depends on the storage coefficient, that is, it decreases for increasing K' (together with an increase of the flood peak attenuation).

- The amount of flood peak attenuation and the size of the near optimal range of reservoir position also depend on the characteristics of extreme precipitation (e.g., the midrange of nearly optimal positions is larger, but the attenuation is smaller, in places where the intensity of rainfall extremes does not vary much with duration, such as the Alps, than in places where it does, such as in central Italy).
- The size of the range of nearly optimal reservoir position does not depend very much on the shape of the catchment (i.e., where the contributing area is concentrated with respect to the outlet section), which has also a limited effect on the amount of flood peak attenuation.
- Using the parsimonious IUH-based method, we also show that the extreme storm duration responsible of the maximum flood peak at the catchment outlet (i.e., the one used in the design storm method; see, e.g., Pilgrim & Cordery, 1993, page 9.13) depends as well on the three nondimensional numbers. Interestingly, by varying A'_R, this critical duration shifts abruptly at the positions in which the flood peak is dominated by the downstream catchment only, by both parts of the catchment, and by the upstream catchment only. This is because our model relates the relevant extreme storm duration to the catchment response time and the latter to catchment area (see, e.g., Gaál et al., 2012).
- Allowing for realistic catchment morphology and nonlinearity in the spillway relationship gives results that are consistent with those obtained analytically using the idealized catchment and the linearity assumption. However, nonlinearity results in a decreasing flood peak attenuation for increasing event return period, as would be expected. Also, and less trivial, nonlinearity results in a slight upstream shift of the optimal reservoir position for increasing event return period; this is because for increasing return period the attenuation of flood quantile due to a given reservoir reduces and the optimal position corresponds to smaller upstream (flood generating) areas.

When compared to existing data-based approaches (e.g., Richter et al., 1996; Wang et al., 2017) or continuous simulation analyses (e.g., Ayalew et al., 2013; Bradley & Potter, 1992), the parsimonious IUH-based method proposed here has two main advantages. First, it can be used for design purposes, for example, for the preliminary investigation of the optimal reservoir position (regardless of its feasibility), size, and spillway for flood risk reduction, without the need to fit very detailed hydrological and reservoir models (which could still be used to then refine the details of design), or to check the effects of reservoirs construction on flood probability distributions at given locations of interest. Second, it can be used for hydrological characterization of catchments at the regional scale. While compact indexes have been used in the literature so far (see, e.g., the reservoir index in Graf, 1999), here the three nondimensional numbers are directly linked to the dominant processes responsible for flood peak attenuation by reservoirs. In other words, the proposed parsimonious IUH-based method is a useful compromise between the detailed models developed for local scale simulation analyses and the descriptive indexes developed for large-scale data-based analyses. The three nondimensional numbers, which can be relatively easily estimated from usually available information on landscape properties and precipitation, could be used to define similarity relationships (in this case between catchments with reservoirs or between different times for one catchment) when analyzing the impact of reservoirs in the reduction of flood peak discharge.

Acknowledgments
The authors would like to thank the associate editor and three anonymous reviewers for their valuable comments and suggestions. M. B. acknowledges the Helmholtz International Fellowship, SYSTEMRISK project (EU grant 676027) for partly funding this work. The Digital Elevation Model (DEM) with grid spacing of 20 × 20 m used in the case study is freely available from ISPRA, http://www.sinanet.isprambiente.it/it/sia-ispra/download-mais/dem20/view.

References

Assani, A. A., Stichelbout, E., Roy, A. G., & Petit, F. (2006). Comparison of impacts of dams on the annual maximum flow characteristics in three regulated hydrologic regimes in Québec (Canada). *Hydrological Processes*, *20*(16), 3485–3501.

Ayalew, T. B., Krajewski, W. F., & Mantilla, R. (2013). Exploring the effect of reservoir storage on peak discharge frequency. *Journal of Hydrologic Engineering*, *18*(12), 1697–1708. https://doi.org/10.1061/(ASCE)HE.1943-5584.0000721

Ayalew, T. B., Krajewski, W. F., & Mantilla, R. (2015). Insights into expected changes in regulated flood frequencies due to the spatial configuration of flood retention ponds. *Journal of Hydrologic Engineering*, *20*(10), 04015010.

Ayalew, T. B., Krajewski, W. F., Mantilla, R., Wright, D. B., & Small, S. J. (2017). Effect of spatially distributed small dams on flood frequency: Insights from the soap creek watershed. *Journal of Hydrologic Engineering*, *22*(7), 04017011.

Batalla, R. J., Gomez, C. M., & Kondolf, G. M. (2004). Reservoir-induced hydrological changes in the Ebro River basin (NE Spain). *Journal of Hydrology*, *290*(1–2), 117–136.

Bradley, A. A., & Potter, K. W. (1992). Flood frequency analysis of simulated flows. *Water Resources Research*, *28*(9), 2375–2385.

Collier, M., Webb, C., & Schmidt, J. (1996). *Dams and rivers: A primer on the downstream effects of dams: Amherst*. Denver: US Geological Survey Circular 1126.

Di Lazzaro, M. (2009). Regional analysis of storm hydrographs in the rescaled width function framework. *Journal of Hydrology*, *373*(3–4), 352–365.

Di Lazzaro, M., Zarlenga, A., & Volpi, E. (2016). Understanding the relative role of dispersion mechanisms across basin scales. *Advances in Water Resources*, *91*, 23–36.

FitzHugh, T. W., & Vogel, R. M. (2011). The impact of dams on flood flows in the United States. *River Research and Applications*, *27*(10), 1192–1215.

Gaál, L., Szolgay, J., Kohnová, S., Parajka, J., Merz, R., Viglione, A., & Blöschl, G. (2012). Flood timescales: Understanding the interplay of climate and catchment processes through comparative hydrology. *Water Resources Research*, *48*, W04511. https://doi.org/10.1029/2011WR011509

Gao, Y., Vogel, R. M., Kroll, C. N., Poff, N. L., & Olden, J. D. (2009). Development of representative indicators of hydrologic alteration. *Journal of Hydrology*, *374*(1–2), 136–147.

Graf, W. L. (1999). Dam nation: A geographic census of American dams and their large-scale hydrologic impacts. *Water Resources Research*, *35*(4), 1305–1311.

Graf, W. L. (2006). Downstream hydrologic and geomorphic effects of large dams on American rivers. *Geomorphology*, *79*(3–4), 336–360.

Gupta, V. K., Waymire, E., & Wang, C. (1980). A representation of an instantaneous unit hydrograph from geomorphology. *Water Resources Research*, *16*(5), 855–862.

Hess, G. W., & Inman, E. J. (1994). *Effects of urban flood-detention reservoirs on peak discharges and flood frequencies, and simulation of flood-detention reservoir outflow hydrographs in two watersheds in Albany Georgia*. Albany, Georgia: US Department of the Interior, US Geological Survey.

Koutsoyiannis, D., Kozonis, D., & Manetas, A. (1998). A mathematical framework for studying rainfall intensity-duration-frequency relationships. *Journal of Hydrology*, *206*, 118–135.

Magilligan, F. J., & Nislow, K. H. (2001). Long-term changes in regional hydrologic regime following impoundment in a humid-climate watershed. *JAWRA Journal of the American Water Resources Association*, *37*(6), 1551–1569.

Magilligan, F. J., & Nislow, K. H. (2005). Changes in hydrologic regime by dams. *Geomorphology*, *71*(1–2), 61–78.

Montaldo, N., Mancini, M., & Rosso, R. (2004). Flood hydrograph attenuation induced by a reservoir system: Analysis with a distributed rainfall-runoff model. *Hydrological Processes*, *18*(3), 545–563.

Nash, J. (1957). The form of the instantaneous unit hydrograph. *IAHS AISH Publication*, *42*, 114–118.

Nehrke, S. M., & Roesner, L. A. (2004). Effects of design practice for flood control and best management practices on the flow-frequency curve. *Journal of Water Resources Planning and Management*, *130*(2), 131–139.

Nilsson, C., & Berggren, K. (2000). Alterations of riparian ecosystems caused by river regulation: Dam operations have caused global-scale ecological changes in riparian ecosystems. how to protect river environments and human needs of rivers remains one of the most important questions of our time. *AIBS Bulletin*, *50*(9), 783–792.

Pegg, M. A., Pierce, C. L., & Roy, A. (2003). Hydrological alteration along the missouri river basin: A time series approach. *Aquatic Sciences*, *65*(1), 63–72.

Pilgrim, D. H., & Cordery, I. (1993). Flood runoff. In D. R. Maidment (Ed.), *Handbook of hydrology* (Vol. 9, 42 pp.). New York: McGraw-Hill Companies.

Poff, N. L., & Zimmerman, J. K. (2010). Ecological responses to altered flow regimes: A literature review to inform the science and management of environmental flows. *Freshwater Biology*, *55*(1), 194–205.

Pringle, C. (2003). What is hydrologic connectivity and why is it ecologically important? *Hydrological Processes*, *17*(13), 2685–2689.

Richter, B. D., Baumgartner, J. V., Braun, D. P., & Powell, J. (1998). A spatial assessment of hydrologic alteration within a river network. *Regulated Rivers: Research & Management*, *14*(4), 329–340.

Richter, B. D., Baumgartner, J. V., Powell, J., & Braun, D. P. (1996). A method for assessing hydrologic alteration within ecosystems. *Conservation biology*, *10*(4), 1163–1174.

Rodriguez-Iturbe, I., & Rinaldo, A. (1997). Fractal river networks: Chance and self-organization.

Rodríguez-Iturbe, I., & Valdes, J. B. (1979). The geomorphologic structure of hydrologic response. *Water Resources Research*, *15*(6), 1409–1420.

Rossi, F., & Villani, P. (1994). A project for regional analysis of floods in Italy, *Coping with floods* (pp. 193–217). Dordrecht: Springer.

Rosso, R. (1984). Nash model relation to horton order ratios. *Water Resources Research*, *20*(7), 914–920.

Ruhi, A., Dong, X., McDaniel, C., Batzer, D., & Sabo, J. (2018). Detrimental effects of a novel flow regime on the functional trajectory of an aquatic invertebrate metacommunity. *Global change biology*, *24*(8), 3749–3765. https://doi.org/10.1111/gcb.14133

Singer, M. B. (2007). The influence of major dams on hydrology through the drainage network of the Sacramento River basin, California. *River Research and Applications*, *23*(1), 55–72.

Walker, K. (1985). A review of the ecological effects of river regulation in Australia, *Perspectives in Southern Hemisphere Limnology* (pp. 111–129). Dordrecht: Springer.

Wang, W., Li, H.-Y., Leung, L. R., Yigzaw, W., Zhao, J., Lu, H., et al. (2017). Nonlinear filtering effects of reservoirs on flood frequency curves at the regional scale. *Water Resources Research*, *53*, 8277–8292. https://doi.org/10.1002/2017WR020871

Williams, G. P., & Wolman, M. G. (1984). Downstream effects of dams on alluvial rivers.

Zhang, Q., Xiao, M., Liu, C.-L., & Singh, V. P. (2014). Reservoir-induced hydrological alterations and environmental flow variation in the East River, the Pearl River basin, China. *Stochastic environmental research and risk assessment*, *28*(8), 2119–2131.